Energy Reports 7 (2021) 5074–5085

Contents lists available at ScienceDirect

Energy Reports

journal homepage: www.elsevier.com/locate/egyr

Research paper

Improve the performance of a semi-active flapping airfoil power generator by adjusting both offsetting mass center displacement and changing pitching axis position

Zhu Jianyang [a,*], Zhu Mingkang [a], Tao Zhang [b]

[a] Institute of Robotics and Intelligent Systems, Wuhan University of Science and Technology, Wuhan, 430081, PR China
[b] Faculty of Engineering and Information Technology, University of Technology Sydney, NSW 2020, Australia

ARTICLE INFO

Article history:
Received 27 February 2021
Received in revised form 23 July 2021
Accepted 3 August 2021
Available online 19 August 2021

Keywords:
Offsetting mass center displacement
Pitching axis position
Power extraction performance
Semi-active flapping airfoil power generator
Promoted to separate
Vortex

ABSTRACT

A comprehensive investigation was carried out in this study, to evaluate the effect of changing pitching axis position and offsetting mass center displacement on the power extraction performance of a semi-active flapping airfoil power generator (FAPG). Unlike previously published literature, the pitching axis position and the mass center position of the airfoil are not to be located at the same position in the current work. A numerical method for accurately simulating the interaction between the fluid and semi-active FAPG was developed and validated to fulfill this objective. The analysis results showed that the optimized pitching axis position and offsetting mass center displacement are found at the value of $d = c/2$ and $x_\theta = -0.15c$ respectively, and compared with the offsetting mass center displacement, the effect of the pitching axis position on the performance of the FAPG is weak. Vortex structure analysis found that the leading-edge vortex is promoted to separate at initial or middle flapping, and it is delayed to separate at down or up flapping, which is the characteristics of the enhanced power extraction performance airfoil.

1. Introduction

Flapping airfoil power generator (FAPG) are promising candidates for low-speed fluid flow power harvesting, due to a number of specific advantages, especially their easily manufacture, highly efficiency and friendly to nature's flying and swimming creatures (Kinsey and Dumas, 2012; Xiao and Zhu, 2014; Xie et al., 2016; Zhu and Tian, 2017; Zhu et al., 2019). However, compared to the traditional rotary turbines, more complex aerodynamic phenomena, such as deep dynamic stall and unsteady leading-edge vortex and trailing edge vortex generating and shedding, are occurring during the flapping of the airfoil. Moreover, the mechanics of how the flapping airfoil extract power from the fluid is still not fully understood, which results in its power extraction performance is currently not comparable with traditional rotary turbines (Rostami and Armandei, 2017; Young et al., 2014; Kinsey et al., 2011).

In general, a flapping airfoil utilized for fluid power harvesting undergoes heaving and pitching motion simultaneously. Based on the activation mechanism of the generator, the FAPGs can be classified into three main categories, which are fully-active system (prescribed both heaving and pitching motion), semi-active system (prescribed pitching and the heaving induced by fluid flow) and fully-passive system (both the pitching and heaving induced by fluid flow) respectively. As discussed by the authors in Filippas et al. (2018) and Shimizu et al. (2008), a semi-active system offers the most feasible model for application due to its wide operation range and simple manufacturing. In addition, most of the early industrial developed FAPGs prototype had used this type of system (Finnigan, 2012; Kloos et al., 2009). Therefore, following this idea, in this work, the performance of this type of FAPGs is investigated.

The power extraction efficiency of the semi-active FAPG, which is defined as the ratio of the net extraction power by the flapping airfoil to the overall swept area free stream power, is used to evaluate the performance of the system quantitatively. It is depending on a widespread parameter space, including the pitching amplitude, active-pitching motion profiles, reduced frequency, pitching axis location, damping and stiffness coefficient, as well as the shape and flexibility of the airfoil etc.

Non-sinusoidal pitching motion profiles have been introduced to improve the efficiency of the semi-active flapping airfoil power harvesting system. Teng et al. (2016) conducted a numerical study to investigate the effect of variation pitching motion profiles on the performance of a semi-active flapping airfoil. In their study, the pitching profile can be changed by adopting different values of β; the pitching profile can gradually change from sinusoidal

* Corresponding author.
E-mail address: zhujy@wust.edu.cn (J. Zhu).

https://doi.org/10.1016/j.egyr.2021.08.024

to a square wave when the value of β changing from zero to ∞. They found the system's power extraction performance can indeed enhance by using non-sinusoidal pitching profile when the pitching amplitude is at a value of 45°. However, when the pitching amplitude is at a value of 75°, the enhancement is limited. Continue the study by Teng et al. (2016), Li et al. (2018) compared the performance of a semi-active flapping airfoil with four different pitching profiles: sinusoidal, sin-like, cosinusoidal and cosine-like. They reported that cosinusoidal pitching motion is more efficient than sinusoidal pitching motion for power harvesting, and cosine-like pitching motion can enhance the harvesting efficiency compared to cosinusoidal pitching motion. Zhu (2019) performed a numerical study to optimize the damping coefficient, spring coefficient and mass ratio on a semi-active flapping airfoil with pitching amplitude of 45°, reduced frequency of 0.32 and Reynolds number of 3400. It was found that the optimal set of spring coefficient is at the value of 1.00, and the variation of mass ratio cannot increase the maximum mean power coefficient and power efficiency of the system, however, it can influence the value of damping coefficient at which the system achieves the maximum mean power coefficient and power efficiency. Besides, it was concluded that reattaching vortex are observed for the airfoil with appropriate damping coefficient, spring coefficient, and mass ratio, which results in the system having better power extraction performance. Zhan et al. (2017) reported that the optimized non-dimensional spring coefficient is 5.0 for a semi-active flapping airfoil to achieve maximum power efficiency at Reynolds number of 1100. Also, the optimized pitching amplitude is depending on the non-dimensional damping coefficient: when the latter is larger than 0.5π, the former is 67.5°; when the latter is at the value of 0.5π, the former is 75°.

Other methods to enhance the power extraction performance of FAPG, which have been conducted in the published paper, include adding a flexible plate attached to the trailing edge of the rigid airfoil, auxiliary smaller flapping airfoils, and two parallel solid walls et al. Wu et al. (2015a) set up a flexible plate attached to the trailing edge of the semi-activated flapping NACA0015 airfoil to improve the power extraction of the system. The results indicated that, because of the increased vortex strength and lift force by the trailing edge plate deformation during the flapping, adding an appropriate flexible plate to the trailing edge of NACA0015 leads to the improvement of the power extraction. Similarly, Liu et al. (2017) designed a flat plate pinned to the trailing edge of a rigid flapping NACA0015 airfoil through a torsional spring to investigate the effect of flexibility on the power extraction performance of the FAPG. It was found that compared to those of a rigid airfoil with a rigid tail, the flexibility can improve the maximum efficiency by 7.24% accompanied by an increasing of mean power coefficient of 6.63%. Liu et al. (2016) used a fully coupled fluid–structure interaction algorithm to study the power extraction performance of a passive flexible flapping airfoil. the results indicated that due to the enhancement of the synchronization between the development of leading-edge vortex and the airfoil deformation, the maximum efficiency is increased by 32.2%. In order to take advantage of the ground effect for efficiency improvement of the FAPG, Wu et al. (2014) arranged a semi-active flapping airfoil near solid walls. They concluded that the performance of the airfoil arrangement in parallel walls is better than it in a side wall. Compared to the situation of free stream, the maximum efficiency can be increased by 27.69% for the airfoil placed between two parallel walls at pitching amplitude of 45° and reduce frequency of 0.2. Further, Wu et al. (2015b) placed two auxiliary smaller airfoils, which rotated about their centers, above and below a main semi-active flapping airfoil, to enhance the power extraction performance of the system. They reported that the vortex around the main flapping airfoil could interact with that shed from the auxiliary airfoils, which results in increased vortex strength and lift force, leads to more fluid power extraction by the main semi-active flapping airfoil, and enhances the maximum efficiency to 120%. Similar to Wu et al. (2015b), Chen et al. (2018) arranged an auxiliary smaller airfoil pitching about its center in the upstream of a main semi-active flapping airfoil. The study was focused on the effect of the distance between two airfoils, the phase difference between the rotating motion and the pitching motion, as well as the frequency of pitching motion. It was found that the introduction of an upstream auxiliary flapping airfoil and its resultant vortex/airfoil interaction can not only increase the primary flapping airfoil power extraction (benefit from the plunging motion), but also reduce the power consumption through the pitching motion. Compared with the single airfoil, the maximum increased efficiency can reach 74%.

Among the performance improving method, changing the pitching axis location is one of the simplest ways to apply in the designing FAPGs prototype. Jamil and Javed (2019) conducted a numerical study to optimize the power extraction performance of a semi-active flapping airfoil based on Theodorsen's 2D thin plate model. It was found that maximum efficiency of 23% is achieved when the system with pitching at the mid chord. Zhu and Peng (2009) numerically investigated the effect of pitching axis location on the power extraction performance of the FAPG. They concluded that the maximum power efficiency is achieved when the pitching axis is close to the center of the hydrodynamic pressure, which is at 0.2–0.5 chord length from the leading edge of the airfoil. While the experimental study by Isogai (2003) and Abiru and Yoshitake (2011) pointed out that the airfoil should be designed that the pitching axis position coincides with the mass center of the wing to obtain the best power extraction performance.

From the above mentioned published papers, it can be concluded that many studies have been carried out to investigate the power extraction performance of the FAPGs. However, few studies have focused the effect of the offsetting pitching axis position and mass center position on the power extraction performance of the FAPGs, while some contrary conclusions are obtained due to many assumptions in the above relation studies. Therefore, this research work accordingly is conducted. In this article, the effects of the offsetting pitching axis position and mass center position on the power extraction performance of a FAPG are analyzed. Based on fluid–structure interaction study, the pitching motion of the airfoil is prescribed, while the heaving motion is determined by the interaction between the fluid and pitching airfoil. Further, it is pertinent to mention here that the performance of the semi-active flapping airfoil, systematically considering the effects of the offsetting pitching axis position and mass center position, is analyzed for the very first time in this work.

2. Principles of the semi-active FAPG

For the semi-active FAPG problem of interest in this study, the schematic principle of the developed prototype is shown in Fig. 1. The rigid, elastically-mounted NACA0015 airfoil is activated to pitch $\theta(t)$ around the Z-axis, and its heaving motion $h(t)$ is induced by the fluid force to heave freely along the Y-axis. The chord length of the airfoil is c, the pitching center o is located by a distance of d from the leading edge of the airfoil, and the pitching axis position and the mass center position (o_i) is not necessary to be at the same location: the interval between the mass center position and pitching axis position is x_θ (also named offsetting displacement), which is positive when the pitching axis is ahead of the mass center. A spring with spring constant K_h coupled with a damper with damping coefficient D_h is employed to represent

the power generator of the turbine. The activated pitching motion of the airfoil is defined as:

$$\theta(t) = -\theta_m \cos(2\pi f t + 0.5\pi) \tag{1}$$

where θ_m is the pitching amplitude, f is the pitching frequency. The passive heaving motion of the airfoil can be derived based on Lagrange's equation.

The general process of the passive heaving motion derivation can be divided into three steps, as shown in Veilleux (2014). First, the kinetic energy P_E and the potential energy K_E of the semi-active flapping airfoil power extraction system need to be found:

$$\begin{aligned} P_E &= P_E(\dot{x}_i, x_i, t) \\ K_E &= K_E(\dot{x}_i, x_i, t) \end{aligned} \tag{2}$$

where x_i is the ith coordinate of the system, the superscript $(\cdot)$ represents derivative with respect to time, t is the time. Second, the Lagrange's equation of the system can be given as:

$$-\frac{d}{dt}\left[\frac{\partial(P_E - K_E)}{\partial \dot{x}_i}\right] + \frac{\partial(P_E - K_E)}{\partial x_i} + F_c = 0 \tag{3}$$

where F_c is the generalized force of the system. The third and last step is to find the specific expression of each item in Eq. (3). To this end, another coordinate system (io_ij) is defined, as shown in Fig. 2, where the arrow direction is the positive direction of the x_θ, r is the mass center position vector, and can be given as:

$$r = mi + nj \tag{4}$$

where

$$m = -x_\theta + x_\theta \cos\theta,\ n = h - x_\theta \sin\theta \tag{5}$$

The relation between coordinate system (io_ij) and coordinate system (XoY) is:

$$\begin{bmatrix} X \\ Y \end{bmatrix} = \begin{bmatrix} i \\ j \end{bmatrix} + \begin{bmatrix} x_\theta \\ 0 \end{bmatrix} \tag{6}$$

Then, the kinetic energy of the components associating of the pitching and the heaving motions of the airfoil (T_P) can be defined as:

$$T_P = \frac{1}{2}\int [(\frac{dm}{dt})^2 + (\frac{dn}{dt})^2]\rho_s dx = \frac{1}{2}(M_P\dot{h}^2 - 2M_P x_\theta \dot{h}\dot{\theta}\cos\theta + M_P x_\theta^2 \dot{\theta}^2) \tag{7}$$

where

$$M_P = \int \rho_s dx \tag{8}$$

and ρ_s is the airfoil mean density.

It is notating that in this work, T_p is equal to P_E, therefore, the expression of potential energy P_E can be defined:

$$P_E = \frac{1}{2}M_P\dot{h}^2 - M_P x_\theta \dot{h}\dot{\theta}\cos\theta + \frac{1}{2}M_P x_\theta^2 \dot{\theta}^2 \tag{9}$$

Since only a spring applied in the heaving direction of the system, the potential energy K_E can be given as:

$$K_E = \frac{1}{2}K_h h^2 \tag{10}$$

Substitution Eqs. (10) and Eq. (9) into Eq. (3), the governing equation for the heaving motion can be described:

$$-\frac{d}{dt}\left[\frac{\partial(\frac{1}{2}M_P\dot{h}^2 - M_P x_\theta \dot{h}\dot{\theta}\cos\theta + \frac{1}{2}M_P x_\theta^2\dot{\theta}^2 - \frac{1}{2}K_h h^2)}{\partial \dot{h}}\right] + \frac{\partial(\frac{1}{2}M_P\dot{h}^2 - M_P x_\theta \dot{h}\dot{\theta}\cos\theta + \frac{1}{2}M_P x_\theta^2\dot{\theta}^2 - \frac{1}{2}K_h h^2)}{\partial h} + F_c = 0 \tag{11}$$

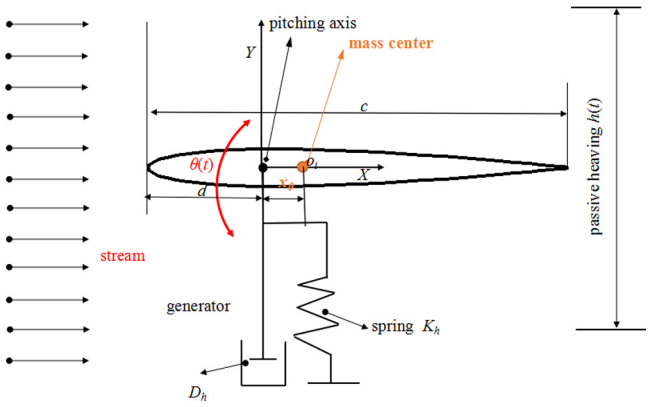

Fig. 1. The schematic principle of the developed prototype FAPG.

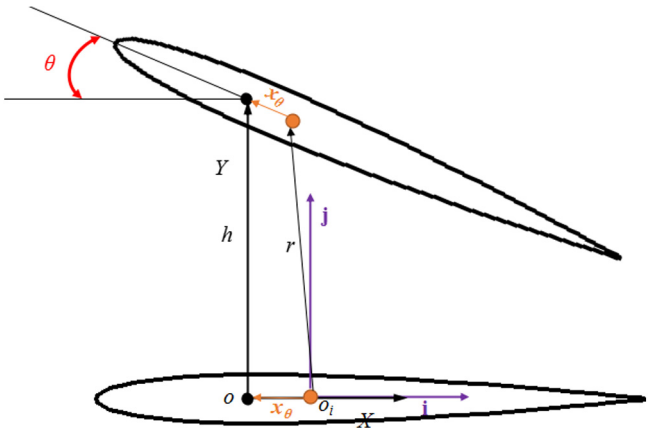

Fig. 2. The coordinates employed for the derivation of the general equations of motion of the semi-active flapping airfoil.

By simplifying Eq. (11), we can get:

$$F_c = M_p\ddot{h} - M_p x_\theta \ddot{\theta}\cos\theta + M_p x_\theta \dot{\theta}^2 \sin\theta + K_h h \tag{12}$$

For the semi-active flapping airfoil (active pitching and passive heaving), F_c is the subtraction of damping force $D_h\dot{h}$ from lift F_Y, therefore, Eq. (12) can be written as:

$$F_Y = M_p\ddot{h} - M_p x_\theta \ddot{\theta}\cos\theta + M_p x_\theta \dot{\theta}^2 \sin\theta + K_h h + D_h\dot{h} \tag{13}$$

where, h, $\dot{h}$, $\ddot{h}$ and F_Y are determined by the interaction between the semi-active flapping airfoil and the fluid flow around the airfoil.

Considering the FAPG in this research, is used to extract wind power at low free stream velocity U_∞. Based on the chord length of the airfoil and wind speed, the Reynolds number of the system is fixed at 1.0×10^4, which is close to the high efficiency flight conditions of the bird and insect (Zhu and Lei, 2018; Sun, 2018). Since FAPG is inspired from the bird and insect's flight, the FAPG working at this range Reynolds number also has better power extraction performance. Therefore, the wind around the airfoil is assumed to be in-compressible, unsteady and viscous laminar flow, and the governing equations are described as:

$$\begin{aligned} \nabla \cdot \vec{V} &= 0 \\ \frac{\partial \vec{V}}{\partial t} + \vec{V}\cdot\nabla\vec{V} &= -\frac{1}{\rho}\nabla p + \nu\nabla^2\vec{V} \end{aligned} \tag{14}$$

where $\vec{V}$ represents the velocity vector, ρ is the wind density, ν is the fluid kinematic viscosity, and p is the pressure.

To fully determine the responding of the semi-active flapping airfoil, some parameters should be defined. The Reynolds number Re, reduced frequency k, damping ratio D^*, spring ratio K^* and mass ratio M^* are given as:

$$Re = \frac{U_\infty c}{\nu}, k = \frac{\pi f c}{U_\infty}, D^* = \frac{D_h}{M_h}, K^* = \frac{1}{2\pi f}\sqrt{\frac{K_h}{M_h}}, M^* = \frac{\rho}{\rho_s} \quad (15)$$

According to the published paper (Zhu, 2019), the spring ratio of 1.0 is set for the system to have better power extraction performance. It was also found in Zhu (2019) that the effect of damping ratio and mass ratio on the power extraction performance of the system are coupled. To simplify the problem in this work, the mass ratio and damping ratio are set at 240 and 2.0 respectively for all the following simulations.

To evaluate the force generation of the system, the lift coefficient C_L, drag coefficient C_D and moment coefficient C_M of the airfoil are given as:

$$C_L = \frac{F_Y}{0.5\rho U_\infty^2 c}, C_D = \frac{F_X}{0.5\rho U_\infty^2 c}, C_M = \frac{M_O}{0.5\rho U_\infty^2 c^2} \quad (16)$$

where, M_O is the aerodynamic torque about pitching center of the airfoil. Note worthily, the force of the airfoil is determined by the effective angle of attack (AOA), which can be defined as:

$$\alpha = \theta(t) - \tan^{-1}(\frac{-\dot{h}}{U_\infty}) \quad (17)$$

To assess the power extraction performance of the system, the mean power coefficient and power efficiency are introduced. For the semi-active flapping airfoil, an external power needs to input the system to drive the pitching motion of the airfoil, and the absorbing power is from the induced heaving motion. Therefore, the mean power coefficient of the system is defined as:

$$\overline{C_P} = \int_0^T C_P dt = \frac{\int_0^T (F_Y\dot{h} - M_O\dot{\theta})dt}{0.5\rho U_\infty^3 c} \quad (18)$$

where, $T = 1/f$ is the pitching cycle, C_P is the net power coefficient of the system. Then, the power efficiency can be defined as:

$$\eta = \overline{C_P}\frac{c}{h_{\max}} \quad (19)$$

where, h_{max} is the overall vertical extent of the airfoil (the distance in Y direction between the highest position and the lowest position reached by the airfoil, either the leading edge or the trailing edge). It can be calculated by:

$$h_{\max} = \max(\text{amplitude}(h+(c-d)\sin(\theta)), \text{amplitude}(h-d\sin(\theta))) \quad (20)$$

3. Numerical method

For the semi-active flapping airfoil studying in this work, there are two models developed to simulate the interaction between the airfoil flapping and wind flow: the aerodynamic and dynamic models. For the aerodynamic model (Eqs. (1) and (14)), the activated pitching motion is employed as input to determine the aerodynamic force of the airfoil. As for the dynamic model (Eq. (13)), the aerodynamic force from the aerodynamic model is applied in Eq. (13) to determine the airfoil heaving motion.

Both the aerodynamic and the dynamic model's simulation are conducted using the commercial computational fluid dynamics (CFD) software Fluent 6.3. The SIMPLE (Semi-implicit method for pressure-linked equations-consistent) is used to deal with the pressure and velocity coupling. The Standard scheme is applied for pressure discretization, and power law scheme is utilized for momentum discretization. The temporal term is discretized using the 1st-order implicit scheme with the dynamic mesh technology employed to realize the airfoil's active pitching and passive heaving.

The discretization of the passive heaving displacement of the airfoil is achieved through the Taylor formula expansion. The heaving displacement of the airfoil at $t+\Delta t$ and $t-\Delta t$ can be given as:

$$\begin{aligned} h^{t+\Delta t} &= h^t + \frac{\dot{h}^t}{1!}\Delta t + \frac{\ddot{h}^t}{2!}(\Delta t)^2 + R_n(\Delta t) \\ h^{t-\Delta t} &= h^t + \frac{\dot{h}^t}{1!}(-\Delta t) + \frac{\ddot{h}^t}{2!}(-\Delta t)^2 + R_n(-\Delta t) \end{aligned} \quad (21)$$

then, the heaving acceleration and velocity of the airfoil at t are given as:

$$\begin{aligned} \ddot{h}^t &= \frac{h^{t+\Delta t} + h^{t-\Delta t} - 2h^t}{\Delta^2 t} \\ \dot{h}^t &= \frac{h^{t+\Delta t} - h^{t-\Delta t}}{2\Delta t} \end{aligned} \quad (22)$$

In order to resolve the numerical instability induced by the low-density ratios, a fictitious mass is added in Eq. (13), then it can be rewritten as:

$$\begin{aligned} F_Y^t + M_p\ddot{h}^{t-\Delta t} &= M_p\ddot{h}^t + M_p\ddot{h}^{t-\Delta t} - M_p x_\theta^t \ddot{\theta}^t \cos\theta^t \\ &+ M_p x_\theta^t \dot{\theta}^{t2} \sin\theta^t + K_h h^t + D_h \dot{h}^t \end{aligned} \quad (23)$$

Substituting Eq. (22) into Eq. (23), we can get the time progressive form of passive heaving displacement of the airfoil:

$$\begin{aligned} h^{t+\Delta t} &= \frac{5M_p - K_h\Delta^2 t}{2M_p + 0.5D_h\Delta t}h^t + \frac{-4M_p + 0.5D_h\Delta t}{2M_p + 0.5D_h\Delta t}h^{t-\Delta t} \\ &+ \frac{M_p}{2M_p + 0.5D_h\Delta t}h^{t-2\Delta t} \\ &+ \frac{(F_Y^t - M_p x_\theta^t(\ddot{\theta}^t\cos\theta^t - \dot{\theta}^{t2}\cos\theta^t))\Delta^2 t}{2M_p + 0.5D_h\Delta t} \end{aligned} \quad (24)$$

During the simulation, the governing equation of active pitching motion as shown in Eq. (1) and the governing equation of passive heaving motion as shown in Eq. (24) are written in C language which is coupled to Fluent 6.3 by using a user-defined function (UDF), and both the active pitching and passive heaving motion are achieved through the dynamic mesh technology.

The computational domain and the grid generating structures are illustrated in Fig. 3. The C-type computational domain which has the outer and inner sub-domains, is employed. The initial position of the pitching center of the airfoil is located at the center of the semi-circle, which has a diameter of $D = 20c$, and the right boundary has a distance of D from the pitching center of the airfoil. Size function is used to mesh the computational domain around the airfoil, which is processed in Gambit. To accurately capture the flow structure around the airfoil, 20 rows of boundary layers are applied to encompass the entire airfoil in the inner domain, and from the airfoil surface, the growth rate of the mesh size is set at 1.1. During the calculating, the inner domain moves according to the airfoil flapping, the grid re-meshing takes place at the interface between the inner and outer domain, and the rest of the outer domain is stationary.

No-slip wall boundary condition is applied at the airfoil surface. The inlet velocity boundary condition which means the wind flow from left to the right is applied at the left, up and down side of the computational domain; the pressure outlet boundary condition is applied at the right side of the computational domain, at which the pressure is set identical to the atmospheric pressure.

Table 1
The grid generation.

Description	Grid nodes on the airfoil	The height of the first cell on the airfoil	Cells in the inner domain	Cells in the outer domain
Grid1	200	$0.001c$	7.6×10^3	1.1×10^4
Grid2	400	$0.0005c$	1.6×10^4	1.1×10^4
Grid3	800	$0.00025c$	3.3×10^4	1.1×10^4
Time step sizes	$\Delta t = T/1000$, $T/2000$ and $T/4000$			

Table 2
The analyzing parameters in typically studied by Wu et al. (2015b).

Names	Values	Names	Values
Reynolds number Re	$Re = 1100$	Pitching axis positions	$d = c/3$
Chord of the airfoil	$c = 0.02$ m	Non-dimensional mass of the airfoil	$M_h/(0.5\rho c^2) = 1.0$
Pitching amplitude	$\theta_m = 30^\circ$	Non-dimensional damping constant	$D_h/(0.5\rho U_\infty c) = \pi$
Offsetting displacement	$x_\theta = 0$	Non-dimensional spring constant	$K_h/(0.5\rho U_\infty^2) = 1.0$

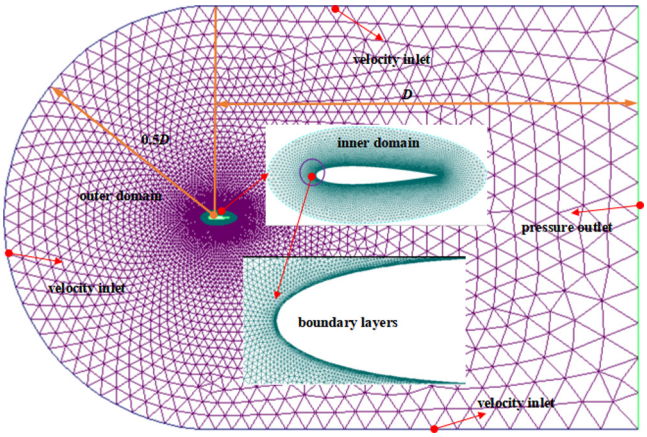

Fig. 3. The computational domain and the grid generating structures.

4. Validation

To ensure the accurately and robustly of the present numerical method for simulating the semi-active flapping airfoil, a typically case with $\theta_m = 70^\circ$, $d = c/3$, $k = 0.075\pi$, $D^* = 2.0$, $K^* = 1.0$, $M^* = 240$, and $x_\theta = 0.0$, is employed to conduct the mesh size and iterate time step sensitively study.

(1) Grid sensitively study

According to the grid generating structures as shown in Fig. 3, the accuracy of the numerical results is determined by two crucial parameters: the height of the first grid layer and the number of nodes distributed on the airfoil surface. Three different grid generating schemes are adapted to investigate the mesh size sensitively, and the details of the grid systems are shown in Table 1.

Fig. 4 demonstrates the instantaneous power coefficient and mean power coefficient of the semi-active flapping airfoil with different grid generating schemes, where the iterate time step is fixed at $\Delta t = T/2000$. The differences of simulation results between the Grid2 and Grid3 are significantly smaller than those between Grid1 and Grid3, which indicates that the solution is convergence at Grid2, and it is employed for further simulation.

(2) Iterate time step sensitively study

Two more iterate time steps are employed to investigate their sensitively. By examining the instantaneous power coefficient and mean power coefficient of the airfoil with different iterate time steps in Fig. 5, it is concluded that the simulation results of the semi-active flapping airfoil with covered three iterate time steps almost have identical value. However, the distinctions of simulation results between the $\Delta t = T/2000$ and $\Delta t = T/4000$ are smaller than those between $\Delta t = T/1000$ and $\Delta t = T/4000$, which indicates that the solution results are not depended on the iterate time step when the iterate time step is smaller than $\Delta t = T/2000$. Therefore, the iterate time step is fixed at $T/2000$ for the following study.

Table 3
The analyzing parameters in typically studied by Kaya et al. (2009).

Names	Values
Reynolds number Re	$Re = 1.0 \times 10^4$
Chord of the airfoil	$c = 1.0$ m
Plunging motion of the airfoil	$h(t) = -0.54\cos(2\pi ft)$
Pitching motion of the airfoil	$\theta(t) = -9.93^\circ \cos(2\pi ft + 84.3^\circ)$
pitching axis positions	$d = c/2$

To validate the proposed methodology, simulation results are needed to compare with the literature results. Accordingly, a typically case studied by Wu et al. (2015b) is implemented as a benchmark. The simulation parameters are set the same as Wu et al. (2015b), as shown in Table 2. Fig. 6 compares the present results with the literature data for the instantaneous lift coefficient and torque coefficient of the airfoil during a steady flapping cycle, and it is found that The lift of the present result is well agreement with the results from Wu et al. (2015b), however, slightly different of the moment coefficients are observed between the present results and the results from Wu et al. (2015b), the reason for this difference may be the different numerical method employed in the present work and literature (Wu et al., 2015b).

To validate the proposed methodology for simulating the aerodynamic performance of the flapping airfoil at Reynolds number of 1.0×10^4, a typically case studied by Kaya et al. (2009) is implemented for comparison. The simulation parameters are set the same as Kaya et al. (2009), as shown in Table 3. It is seen from Fig. 7 that the results of the present numerical method and literature data agree very well, which indicates that the proposed methodology can accurately simulate the aerodynamic performance of the flapping airfoil at Reynolds number of 1.0×10^4.

5. Results and discussion

In the current work, the effect of the offsetting mass center displacement and pitching axis position on the power extraction performance of the FAPG are systematically investigated. For all the cases, the pitching amplitude θ_m, Reynolds number Re, and reduced frequency k are set to be 70°, 1.0×10^4, and 0.075π respectively. Four distinct pitching axis positions ($d = c/4$, $c/3$, $c/2$,

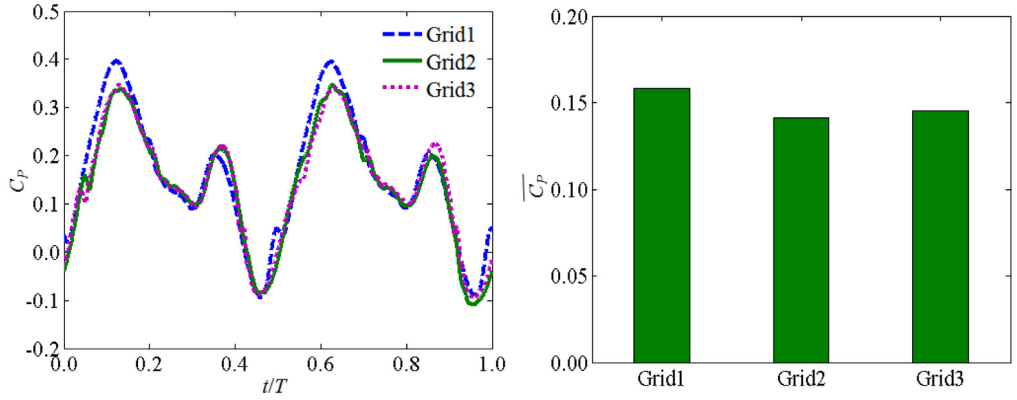

Fig. 4. The instantaneous power coefficient and mean power coefficient of semi-active flapping airfoil with different grid generating schemes.

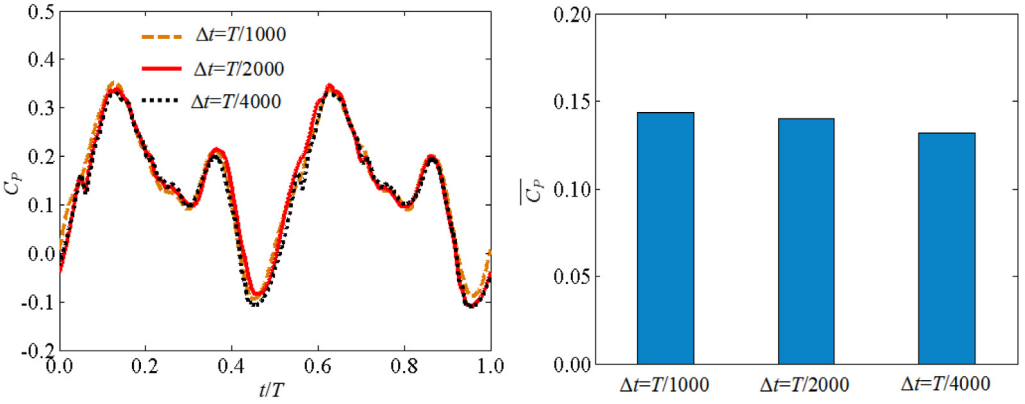

Fig. 5. The instantaneous power coefficient and mean power coefficient of semi-active flapping airfoil with different iterate time steps schemes.

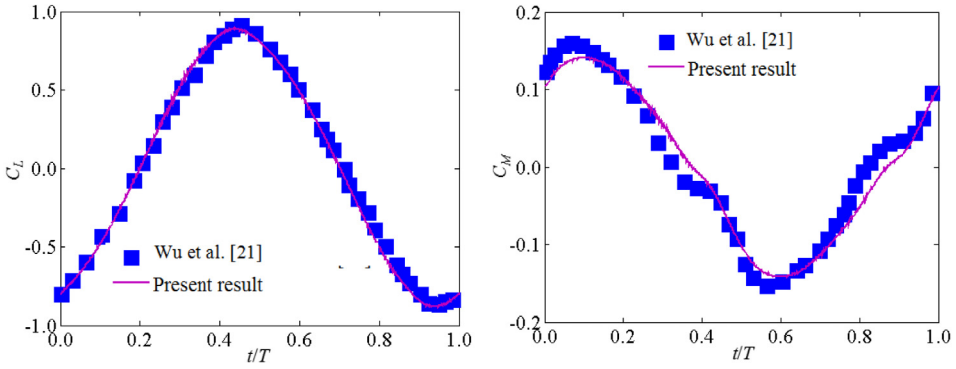

Fig. 6. Comparison of the results of instantaneous and mean power coefficient for the semi-active flapping airfoil: present numerical data VS literature data.

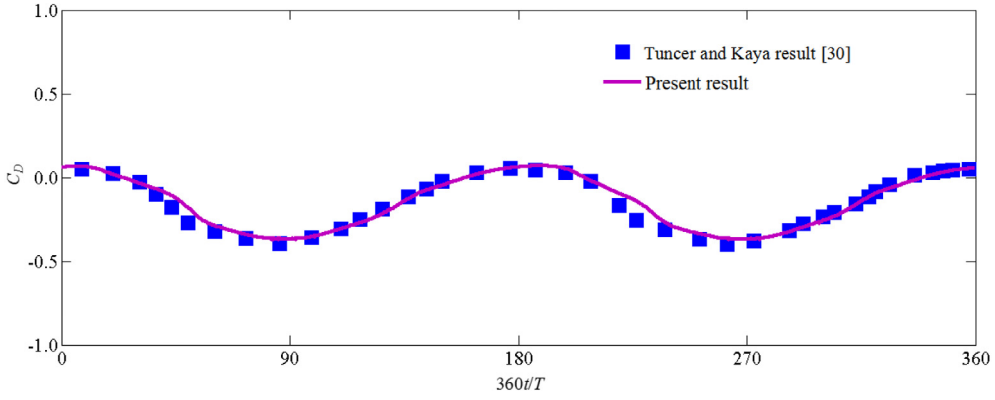

Fig. 7. Comparison of the results of instantaneous drag coefficient for the flapping airfoil: present numerical data VS literature data.

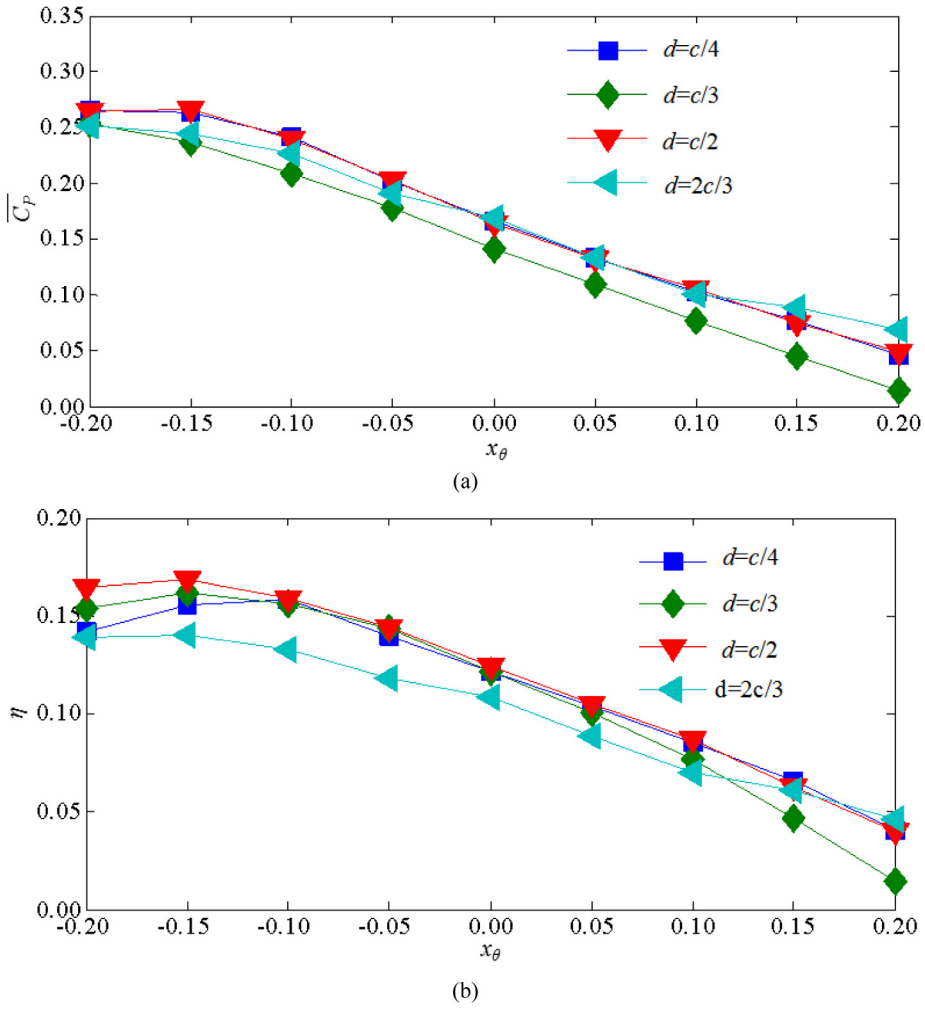

Fig. 8. The performance of the FAPGs with different pitching axis position and offsetting displacement: (a) mean power coefficient; (b) efficiency.

$2c/3$) are considered, for each of them, and the distances between the mass center position and their corresponding pitching axis position (x_θ - offsetting displacement) are evaluated from $-0.20c$ to $0.20c$ with an interval of $0.05c$.

5.1. The mean power coefficient and efficiency

The mean power coefficient and efficiency of the FAPG with different pitching axis position and offsetting displacement are compared directly to illustrate the advantage of FAPG applied offsetting pitching displacement and changing pitching axis position. Fig. 8 manifested that the pitching axis position and offsetting displacement can influence the performance of the FAPGs significantly.

Generally, compared with the FAPGs with zero offsetting displacement ($x_\theta = 0.0$), both of the mean power coefficient and efficiency are enhanced with negative offsetting displacement. And for the covered FAPGs, the maximum mean power coefficient and efficiency are achieved with $x_\theta = -0.15c$ and $d = c/2$, at which 62% more mean power coefficient and 35% more efficiency than with $x_\theta = 0.00c$ and $d = c/2$ are obtained. On the other hand, when the FAPGs are applied positive x_θ, both of the mean power coefficient and efficiency are deteriorated.

With focused on the pitching axis position influence, it is found that when the FAPGs with negative x_θ, the FAPGs with $d = c/2$ has larger mean power coefficient and also the efficiency than the other FAPGs no matter the negative x_θ is, which indicates that the optimized pitching axis position is at $d = c/2$ for the FAPGs studied in this work. Moreover, compared with the offsetting displacement, the influence of the pitching axis position on the performance of the FAPG is weak, since the maximum difference of the efficiency caused by employed different pitching axis position is 16.71% (between the FAPG with $d = c/2$ and $2c/3$).

With focused on offsetting displacement influence, it is found that both the mean power coefficient and efficiency are changing slightly with the x_θ increasing, when the x_θ is at the range of $-0.20c \sim -0.15c$, and they decrease monotonously when the x_θ is larger than $-0.10c$. The optimized offsetting displacement is found at $x_\theta = -0.15c$, where the FAPGs have maximum efficiency, except for the FAPG with $d = c/4$ while the optimized offsetting displacement is at $x_\theta = -0.10c$. Nevertheless, the efficiency difference of this FAPG with $x_\theta = -0.10c$ and $-0.15c$ is less than 2%. From this analysis, it is concluded that the optimized offsetting displacement is found at $x_\theta = -0.15c$ for the covered FAPGs in this work.

5.2. Effect of pitching axis position

To explore how the pitching axis position influences the performance of the FAPG in details, two FAPGs with $d = c/2$ and $2c/3$ are selected for instance, and for the cases studied in this section, the offsetting displacement is fixed at $x_\theta = -0.15c$.

The time history of the passive heaving velocity, lift coefficient, moment coefficient and power coefficient with different pitching

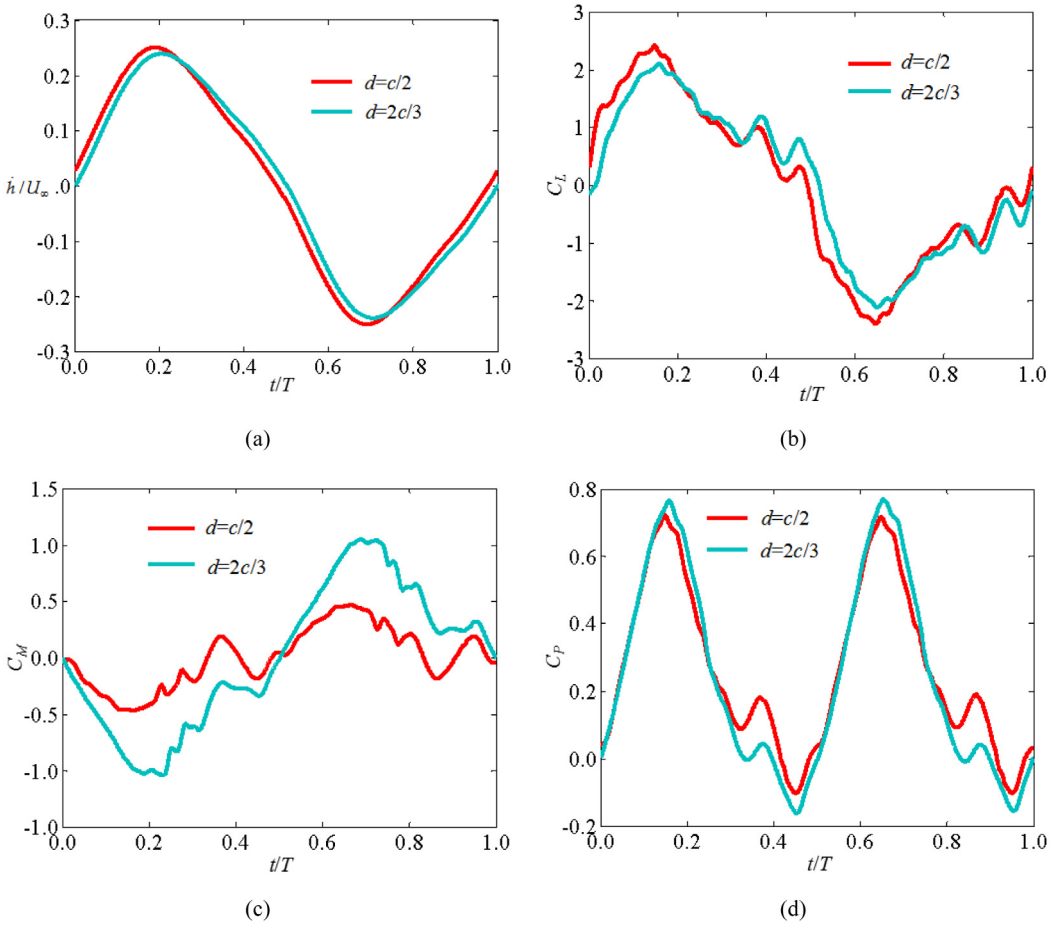

Fig. 9. The time history of the passive heaving velocity, lift coefficient, moment coefficient and power coefficient with different pitching axis position: (a) passive heaving velocity; (b) lift coefficient; (c) moment coefficient; (d) power coefficient.

axis position is illustrated in Fig. 9. As shown in Fig. 9(a) and (b), the variation of passive heaving velocity and lift coefficient are mainly affected by the pitching axis position in the form of peak value, the FAPG with $d = c/2$ has slightly larger passive heaving velocity and lift coefficient amplitude than the FAPG with $d = 2c/3$, which results in almost identical power extraction from the induced heaving motion for the two studied FAPGs. On the other hand, it is seen from Fig. 9(c) that the variation of moment coefficient is also primarily affected by the pitching axis position in the form of the peak value. Smaller moment coefficient almost during the whole flapping cycle is observed for the FAPG with $d = c/2$, which indicates that smaller external power needs to input the system to drive the pitching motion of the airfoil if the FAPG has a pitch axis position of $d = c/2$.

It is well known that for the semi-active FAPG, the power extracted from the fluid is mainly by the lift-driven passive heaving motion, and the effective angle of attack determines the lift of the airfoil. Therefore, the time variation of the effective angle of attack for the FAPGs with different pitching axis position is presented in Fig. 10(a). It is found that the two curves almost coincide with each other, which is the reason for the FAPGs with $d = c/2$ and $2c/3$ almost having identical lift coefficient as shown in Fig. 9(b).

According to Eq. (19), besides the power coefficient, the efficiency of the system is also affected by the h_{max}. In this section, it is found that h_{max} is determined by the Leading edge of the airfoil. Fig. 10(b) shows the time history of the leading edge displacement of the airfoil (h_{lead}) with different pitching axis position. Obviously, the peak h_{lead} of the FAPG with $d = 2c/3$ is slightly larger than the FAPG with $d = c/2$, and this is another reason for the FAPG with $d = 2c/3$ has a lower efficiency than the FAPG with $d = c/2$.

The instantaneous vortex contours of the above-conducted cases for a single flapping cycle are presented in Fig. 11. Similar vortex structures are observed around the two FAPGs with different pitching axis position. However, at $t = 0.00T$ and $0.50T$, when the airfoil has maximum pitching velocity, obviously the leading vortex of the airfoil is delayed to separate from the airfoil surface for the FAPGs with $d = 2c/3$, which is the reason for the FAPGs with $d = 2c/3$ has more significant moment coefficient.

5.3. Effect of offsetting displacement

The effect of offsetting displacement on the power extraction performance of FAPG is further analyzed in this section. Again, two typically FAPGs with $x_\theta = -0.15c$ and $0.00c$ are selected for instance, and for the cases studied in this section, the pitching axis position is fixed at $d = c/2$.

The time history of the passive heaving velocity, lift coefficient, moment coefficient and power coefficient with different offsetting displacement is illustrated in Fig. 12. It is seen from this figure that the time variation curves of the lift coefficient and moment coefficient of the two studied FAPGs are almost overlapping with each other, which indicates that these two parameters are affected by the offsetting displacement slightly. However, on the other hand, as shown in Fig. 12(a), the time variation of passive heaving velocity is affected by the offsetting displacement significantly in the form of amplitude, the FAPG

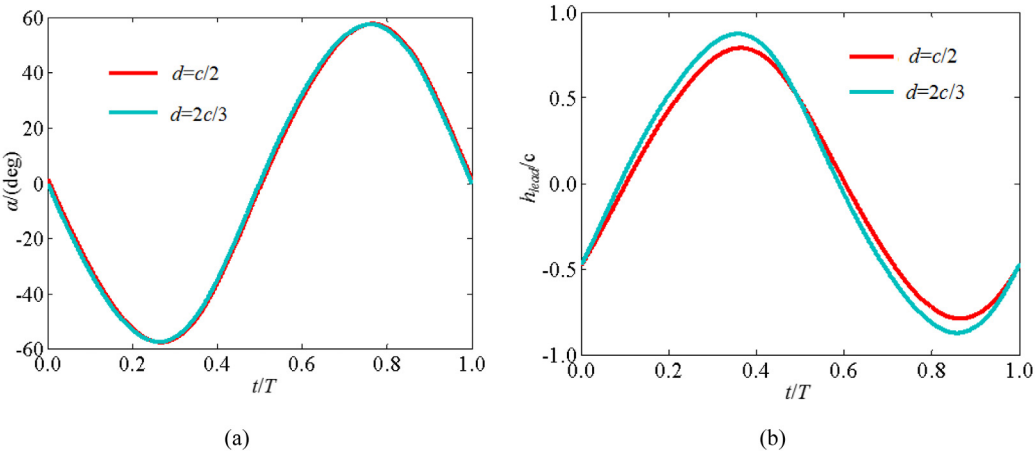

Fig. 10. The time history of the effective angle of attack and leading edge displacement of the airfoil with different pitching axis position: (a) effective angle of attack; (b) leading edge displacement of the airfoil.

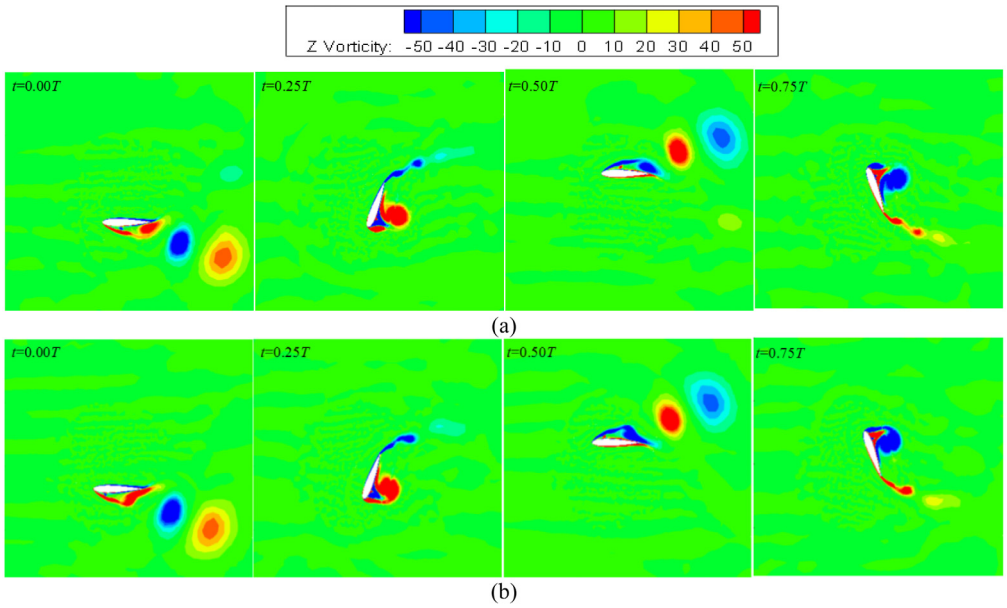

Fig. 11. The instantaneous vortex contours of the FAPG with different pitching axis position for a single flapping cycle: (a) $d = c/2$; (b) $d = 2c/3$.

with $x_\theta = -0.15c$ has larger passive heaving velocity than the FAPG with $x_\theta = 0.00c$ almost during the whole flapping cycle, which results in the FAPG with $x_\theta = -0.15c$ has larger power coefficient, as shown in Fig. 12(d).

Fig. 13(a) plots the time history of the effective angle of attack of the FAPG with different offsetting displacement. It is found that the offsetting displacement can influence the peak value of the effective angle of attack, the FAPG with $x_\theta = -0.15c$ has a smaller effective angle of attack peak than the FAPG with $x_\theta = -0.00c$. As well known that the effective angle of attack can influence the lift of the airfoil significantly, while in this work, it is shown that although the FAPG with $x_\theta = -0.15c$ has smaller effective angle of attack peak than the FAPG with $x_\theta = -0.00c$, the lift coefficient of the two FAPGs almost have identical amplitude, which indicates that the effective angle of attack is not the main influences factors on the power extraction of the FAPG studied in this work.

Fig. 13(b) illustrates the leading edge displacement of the airfoil with different offsetting displacement. The time variation of leading edge displacement of the airfoil is affected by the offsetting displacement not only in the form of peak value but also the phase difference. There is a phase delay for the FAPG with $x_\theta = -0.15c$ to achieve maximum or minimum leading edge displacement amplitude, although the FAPG with $x_\theta = -0.15c$ has a larger amplitude than the FAPG with $x_\theta = 0.00c$.

From the above analyzing, it is noting that the effect of offsetting displacement on the power extraction performance of FAPG are: (a) changing the phase angle between the pitch and heave motion; (b) increasing the heave amplitude, both of which increase the heave velocity and thus power. Those results indicates that offsetting mass center displacement is a clever way to reproduce a wider variety of kinematics into semi-passive motion of flapping airfoil.

Fig. 14 shows the instantaneous vortex contours of the above-conducted cases for a single flapping cycle. It is seen from this figure that the offsetting displacement can influence the vortex structure of the airfoil during the whole flapping cycle, at $t = 0.00T$ and $t = 0.50T$, due to the airfoil applied to offset displacement, the leading-edge vortex is promoted to separate from the airfoil surface. In contrast, at down or up flapping, the leading edge vortex of the FAPG with $x_\theta = -0.15c$ is closer to the airfoil

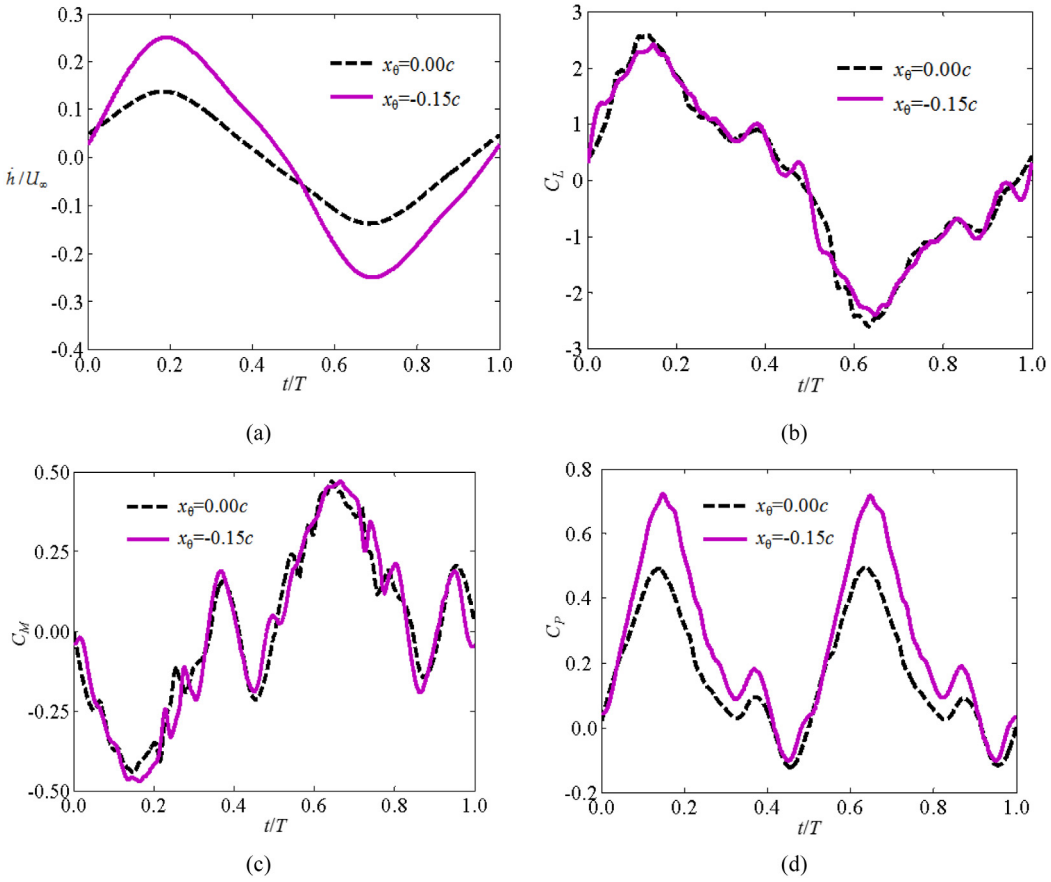

Fig. 12. The time history of the passive heaving velocity, lift coefficient, moment coefficient and power coefficient with different offsetting displacement: (a) passive heaving velocity; (b) lift coefficient; (c) moment coefficient; (d) power coefficient.

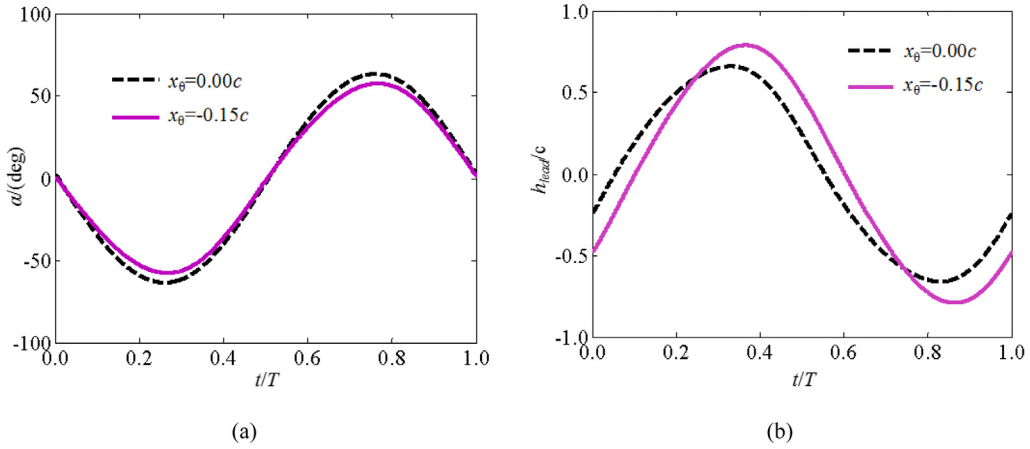

Fig. 13. The time history of the effective angle of attack and leading edge displacement of the airfoil with different offsetting displacement: (a) effective angle of attack; (b) leading edge displacement of the airfoil.

surface, which indicates that the leading vortex of the airfoil is delayed to separate from the airfoil surface.

6. Conclusion

A comprehensive investigation was carried out to find the desirable pitching axis position and offsetting displacement for the semi-active FAPG. Different from previously published literature, the pitching axis position and the mass center position of the airfoil is not to be located at the same position at this work. A numerical method based on unsteady Navier–Stokes equations, prescribed pitching equation and passive heaving equation of the airfoil is developed and validated to simulate the interaction between fluid and semi-active FAPG accurately. Four different pitching axis position are investigated, and for each of them, the distance between the mass center position and pitching axis position (x_θ offsetting displacement) are evaluated from $-0.20c$ to $0.20c$ with an interval of $0.05c$. The main conclusions of this work are summarized as:

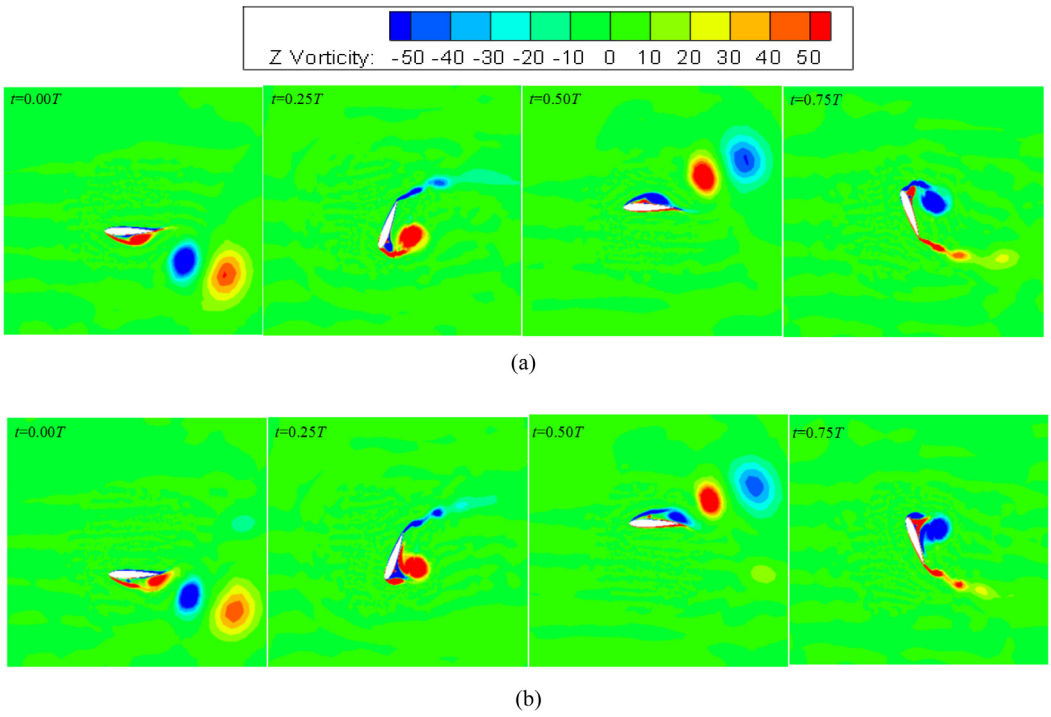

Fig. 14. The instantaneous vortex contours of the FAPG with different offsetting displacement for a single flapping cycle: (a) $x_\theta = 0.00c$; (b) $x_\theta = -0.15c$.

(1) Effect of pitching axis position: the optimized pitching axis position is found at $d = c/2$ for the semi-active FAPGs studied in this work;
(2) Effect of offsetting displacement: the optimized offsetting displacement is found at $x_\theta = -0.15c$ for the covered semi-active FAPGs in this work. Compared with the FAPGs with zero offsetting displacement ($x_\theta = 0.0$), both the mean power coefficient and efficiency are enhanced for the FAPGs applied negative offsetting displacement. For the covered FAPGs, the maximum mean power coefficient and efficiency is achieved for the FAPG with $x_\theta = -0.15c$ and $d = c/2$, at which 62% more mean power coefficient and 35% more efficiency than the FAPG with $x_\theta = 0.00c$ and $d = c/2$ are obtained.
(3) Compared with the offsetting displacement, the effect of the pitching axis position on the performance of the FAPG is weak, since the maximum difference of the efficiency caused by employed different pitching axis position is 16.71% (between the FAPG with $d = c/2$ and $2c/3$).
(4) The vortex structure of the airfoil shows that pitching axis position and offsetting displacement can influence the leading-edge vortex forming and shedding process. The vortex characteristics of the enhanced power extraction performance airfoil are: at initial or middle flapping cycle, the leading-edge vortex should separate from the airfoil surface quickly, while at down or up flapping, the leading-edge vortex should delay separating from the airfoil surface.

It is worth noting that changing the pitching axis position and offsetting displacement is the simplest and most economical way to improve the performance of a FAPG, and it is convenient for the engineers to update their prototypes easily. However, the conclusion obtained in this work are based on the specific parameter range and two dimension numerical simulation, in the future work, wide parameter range and three dimension numerical simulation investigating are needed to be carried out.

Data accessibility

The data supporting this article will be available upon request.

CRediT authorship contribution statement

Zhu Jianyang: Modeling and simulation, Calculations. **Zhu Mingkang:** Writing - original draft, Writing - review & editing. **Tao Zhang:** Conceptualization, Writing - original draft, Writing - review & editing.

Declaration of competing interest

The authors declare that they have no known competing financial interests or personal relationships that could have appeared to influence the work reported in this paper.

Acknowledgment

This work was supported by National Natural Science Foundation of China (project No. 51975429, 51505347), and Wuhan Application Foundation Frontier Project, China (2019010701011404).

References

Abiru, H., Yoshitake, A., 2011. Study on a flapping wing hydroelectric power generation system. J. Environ. Eng. 6, 178–186.
Chen, Y., Nan, J., Wu, J., 2018. Wake effect on a semi-active flapping foil based energy harvester by a rotating foil. Comput. Fluids. 160, 51–63.
Filippas, E.S., Gerostathis, T.P., Belibassakis, K.A., 2018. Semi-activated oscillating hydrofoil as a nearshore biomimetic energy system in waves and currents. Ocean Eng. 154, 396–415.
Finnigan, T.D., 2012. Device for capturing energy from a fluid flow. U.S. Patent 8, 288, 883.
Isogai, K., 2003. Design study of elastically supported flapping wing power generator. In: Int. Forum Aeroelasticity Struct. Dyn. Amsterdam, 2003.
Jamil, M., Javed, A., 2019. Design optimization of a semi-active flapping foil in an energy extraction mode. In: 2019 Int. Conf. Eng. Emerg. Technol. IEEE, pp. 1–8.

Kaya, M., Tuncer, I.H., Jones, K.D., et al., 2009. Optimization of flapping motion parameters for two airfoils in a biplane configuration. J. Aircr. 46, 583–592.
Kinsey, T., Dumas, G., 2012. Computational fluid dynamics analysis of a hydrokinetic turbine based on oscillating hydrofoils. J. Fluids Eng. Asme. 134 (2), 021104.
Kinsey, T., Dumas, G., Lalande, G., et al., 2011. Prototype testing of a hydrokinetic turbine based on oscillating hydrofoils. Renew. Energy 36, 1710–1718.
Kloos, G., Gonzalez, C.A., Finnigan, T.D., 2009. The bioSTREAM tidal current energy converter. In: Eur. Wave Tidal Conf. EWTEC. Uppsala, Sweden. pp. 426–433.
Li, W., Wang, W.-Q., Yan, Y., Tian, F.-B., 2018. Effects of pitching motion profile on energy harvesting performance of a semi-active flapping foil using immersed boundary method. Ocean Eng. 163, 94–106.
Liu, Z., Tian, F.B., Young, J., et al., 2017. Flapping foil power generator performance enhanced with a spring-connected tail. Phys. Fluids 29, 123601.
Liu, W., Xiao, Q., Zhu, Q., 2016. Passive flexibility effect on oscillating foil energy harvester. AIAA J. 54, 1172–1187.
Rostami, A.B., Armandei, M., 2017. Renewable energy harvesting by vortex-induced motions: Review and benchmarking of technologies. Renew. Sustain. Energy Rev. 70, 193–214.
Shimizu, E., K. Isogai, K., Obayashi, S., 2008. Multiobjective design study of a flapping wing power generator. J. Fluids Eng. 130, 021104.
Sun, M., 2018. Aerodynamics of animal flight. Acta Aerodyn. Sin. 36, 122–128.
Teng, L., Deng, J., Pan, D., Shao, X., 2016. Effects of non-sinusoidal pitching motion on energy extraction performance of a semi-active flapping foil. Renew. Energy. 85, 810–818.
Veilleux, J.-C., 2014. Optimization of a Fully-Passive Flapping-Airfoil Turbine. Université Laval.
Wu, J., Chen, Y.L., Zhao, N., 2015b. Role of induced vortex interaction in a semi-active flapping foil based energy harvester. Phys. Fluids. 27, 93601.
Wu, J., Qiu, Y.L., Shu, C., Zhao, N., 2014. Pitching-motion-activated flapping foil near solid walls for power extraction: A numerical investigation. Phys. Fluids. 26, 83601.
Wu, J., Wu, J., Tian, F.-B., Zhao, N., Li, Y.-D., 2015a. How a flexible tail improves the power extraction efficiency of a semi-activated flapping foil system: A numerical study. J. Fluids Struct. 54, 886–899.
Xiao, Q., Zhu, Q., 2014. A review on flow energy harvesters based on flapping foils. J. Fluids Struct. 46, 174–191.
Xie, Y.H., Jiang, W., Lv, K., 2016. Review on research of flapping foil for power generation from flow energy. Proc. CSEE. 36, 5564–5574.
Young, J., Lai, J.C.S., Platzer, M.F., 2014. A review of progress and challenges in flapping foil power generation. Prog. Aerosp. Sci. 67, 2–28.
Zhan, J., Xu, B., Wu, J., Wu, J., 2017. Power extraction performance of a semi-activated flapping foil in gusty flow. J. Bionic Eng. 14, 99–110.
Zhu, J., 2019. The effect of damping coefficient, spring coefficient, and mass ratio on the power extraction performance of a semiactive flapping wing. Int. J. Aerosp. Eng. 2019.
Zhu, J., Lei, B., 2018. Effect of wing-wing interaction on the propulsive performance of two flapping wings at biplane configuration. Appl. Bionics Biomech. 8901067, 1–12.
Zhu, Q., Peng, Z., 2009. Mode coupling and flow energy harvesting by a flapping foil. Phys. Fluids. 21, 33601.
Zhu, J., Tian, T., 2017. The time asymmetric pitching effects on the energy extraction performance of a semi-active flapping wing power generator. Eur. J. Mech. 66, 92–101.
Zhu, B., Xia, P., Huang, Y., Zhang, W., 2019. Energy extraction properties of a flapping wing with an arc-deformable airfoil. J. Renew. Sustain. Energy. 11, 23302.